IOPscience iopscience.iop.org

Home Search Collections Journals About Contact us My IOPscience

Time series analysis of the synchronization mismatch in two coupled one-dimensional lattices of phase oscillators

This article has been downloaded from IOPscience. Please scroll down to see the full text article.

2002 J. Phys.: Condens. Matter 14 2257

(http://iopscience.iop.org/0953-8984/14/9/314)

View the table of contents for this issue, or go to the journal homepage for more

Download details:
IP Address: 171.66.16.27
The article was downloaded on 17/05/2010 at 06:15

Please note that terms and conditions apply.

INSTITUTE OF PHYSICS PUBLISHING JOURNAL OF PHYSICS: CONDENSED MATTER

J. Phys.: Condens. Matter **14** (2002) 2257–2263 PII: S0953-8984(02)31190-1

Time series analysis of the synchronization mismatch in two coupled one-dimensional lattices of phase oscillators

Carlos L Pando L

Universidad Autónoma de Puebla, Instituto de Fisica, Apdo. Postal J-48, Puebla, Pue 72570, México

E-mail: carlos@sirio.ifuap.buap.mx

Received 23 November 2001
Published 22 February 2002
Online at stacks.iop.org/JPhysCM/14/2257

Abstract

We study a model that consists of two identical unidirectionally coupled one-dimensional arrays of chaotic phase oscillators. The time series (TS) of the distance between the arrays is analysed. The probability distribution functions (PDFs) of these distances typically display tails with power-law dependence. The autocorrelation function and the PDF of the laminar phases of these TS depend strongly on the stroboscopic section.

1. Introduction

Chaotic behaviour means that two trajectories starting from slightly different initial conditions diverge exponentially as time goes on [1]. An important result is that the trajectories of chaotic systems can be synchronized if they are suitably coupled together [2]. It has been found that chaotic synchronization between two identical subsystems is a canonical example where on–off intermittency can take place [2]. On–off intermittency is observed when chaotic motion on an invariant manifold loses its stability when a control parameter is changed [3]. In the synchronization of identical chaotic systems, the invariant manifold is the state where the variables of the subsystems have the same values all the time. In on–off intermittency, the system spends long periods of time in the vicinity of the invariant manifold. These intervals are interrupted by short bursts where the system moves away from the invariant manifold [3]. The field of chaos synchronization is a multidisciplinary field of research with several interesting applications [4].

The problem of synchronization between single arrays has received special attention in the last few years. For instance, chaotic synchronization between two one-dimensional (1D) lattices of oscillators has been considered [5]. We mainly study the time series (TS) of the distance between two coupled 1D arrays. In the context of chaotic synchronization, the kind of intermittency that we find in our model shows properties that differ from those observed in on–off intermittency.

 © 2002 IOP Publishing Ltd Printed in the UK

2. The model

Here, we describe the model of two coupled 1D arrays of limit-cycle oscillators. The configuration of this model is known as the master–slave configuration. The model reads

$$\begin{aligned} \frac{\mathrm{d}\theta_j}{\mathrm{d}t} &= \beta K[\sin(\theta_{j-1}-\theta_j)+\sin(\theta_{j+1}-\theta_j)] \\ \frac{\mathrm{d}\phi_j}{\mathrm{d}t} &= \beta K[\sin(\phi_{j-1}-\phi_j)+\sin(\phi_{j+1}-\phi_j)]+\Gamma[\sin(\theta_j-\phi_j)] \end{aligned} \tag{1}$$

where $j = 1, N$, θ_j and ϕ_j are the phases of the master and slave arrays respectively, and t represents time. $K = 1$ if $iT \leqslant t < iT+T$ and $K = -1$ if $iT+T \leqslant t < (i+2)T$, where i is an even integer and $2T$ is the period of modulation; that is, the factor K is a periodic step function. For the sake of definition, we have set $T = 1$. β is the coupling between the oscillators along the 1D array, and Γ is the coupling constant across the arrays. The typical parameters for the model are: $N = 33$; $\beta = 20.0$; $\Gamma \sim 17.0$. For the aforementioned parameters, the change of sign of the coupling βK leads to spatio-temporal chaos (STC) where a typical trajectory in each 1D array oscillates between a sink and a node whose stability alternates [6]. The behaviour of the master array in equation (1) is qualitatively similar to its discrete-time version [6]. Physically, equation (1) describes a system of 1D arrays of phase-locked loops (PLL). These are electric circuits where the variables are on tori of dimension N [7]. We underline that Poincaré sections which differ by a phase T are symmetric. We will define a stroboscopic section along the time axis. The phase of this section is given by the number τ, where $\tau = t \pmod{T}$, $jT \leqslant t < jT + T$, and j is an integer.

3. Statistics of the transverse fluctuations

Now we study the statistical distribution of the transverse fluctuations H. These are defined as $H_n = \left(\sum_{j=1}^{j=N} \sqrt{[\sin(\theta_j-\phi_j)]^2+[1-\cos(\theta_j-\phi_j)]^2}\right)/N$. This is the distance between the two arrays. H is a continuous-time function, while H_n represents the values of H at times where $\tau = t \pmod{T}$.

3.1. The section at $\tau = 0$

In order to have a framework to compare the different sections τ, let us first consider in detail the section at $\tau = 0$. We have studied the TS of $\log_{10} H_n$ for three different values of Γ. For $\Gamma = 9$ the TS has been characterized as a first-order Markov process with two symbols. However, as Γ becomes larger, this description is no longer useful.

In figure 1 we show the probability distribution functions (PDFs) evaluated numerically for the TS described above. The data set for each TS consists of 2×10^6 points. We clearly observe that for $\Gamma = 15$ and 17 there is only a single large hump. Instead, for $\Gamma = 9$ there are two humps which account for the Markovian description. The PDF for $\log_{10}(H_n)$ with $\Gamma = 17$ can be approximated using a hyperbolic PDF [8]. This is displayed in figure 1(c) (long dashed curves). A hyperbolic distribution P is defined as $\log_{10}(P) = [-a\sqrt{\delta^2+(x-\mu)^2}+b(x-\mu)]+\log_{10}(C)$, where C is a normalization factor. In our case, $x = \log_{10} H(t)$ and the PDF parameters are $a = 1.11$, $b = 0.238$, $\delta = 1.437$ and $\mu = -7.88$. Barndorff and Nielsen introduced the hyperbolic PDF in 1977 motivated by the study of statistical laws in geology. These PDFs also found applications in turbulence and finance [8]. The asymptotes of this PDF are given by $-a|x-\mu|+b(x-\mu)$. It is clear that in the region where the asymptotes prevail, the respective PDF $\tilde{P}$ of H_n has power-law tails, i.e. there are right and left tails with a power-law dependence. However, this does not

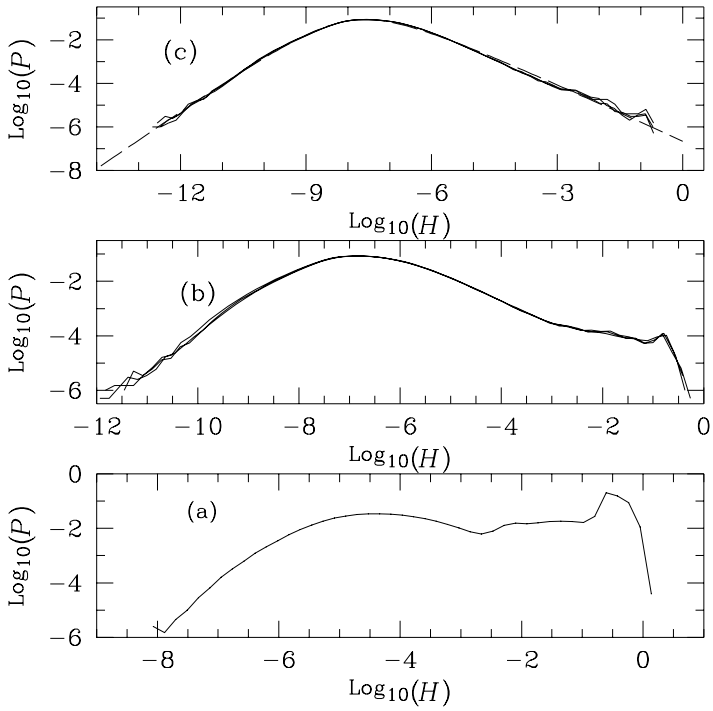

Figure 1. Plot of $\log_{10} P$ versus $\log_{10} H_n$ with $\tau = 0$, $N = 33$ and $\beta = 20.0$ for (a) $\Gamma = 9$, (b) $\Gamma = 15$ and (c) $\Gamma = 17$. The dashed curve represents the hyperbolic PDF.

indicate any eventual divergence since the argument of the PDF $\tilde{P}$ is bound to be due to the finite size of H_n; that is, the PDF $\tilde{P}$ behaves as a truncated Levy distribution law for extreme values [8]. The most probable value of H_n, which we label H_{mp}, is found from the equation $\mathrm{d}P/\mathrm{d}H_n = 0$ [8]. For $H_n \gg H_{mp}$, the right tail of the PDF $\tilde{P}$ of H_n is given by $\tilde{P} \sim H_n^{-0.87}$, while for $H_n \ll H_{mp}$, the left tail of the PDF of H_n is given by $\tilde{P} \sim H_n^{1.34}$. For comparison, we mention that the distance r between two coupled 1D maps has a PDF that has a power-law form for small r while it decays like $\exp(-\alpha r^2)$ for large r [2]. The functional form of the latter contrasts not only with the PDF $\tilde{P}$ of H_n at $\tau = 0$ but with all PDFs at $\tau \neq 0$, as we see below.

Another useful quantity to characterize the TS is given by the moments of order p:$D(\kappa, p) = \langle |H_{n+\kappa} - H_n|^p \rangle$ where $\langle \cdots \rangle$ represents the statistical average of H_n. After some suitable p-dependent shift, $D(\kappa, p)$ is plotted in figure 2(a). We do not see any clear-cut scaling region which would define a set of Hurst exponents [8]. Instead, what we see is that as κ increases, $D(\kappa, p)$ saturates for all moments p. This suggests that the data set of the TS given by $\sigma(\kappa) = \log_{10}(H_{n+\kappa}/H_n)$ tends to converge to a single PDF as κ is increased. This is indeed what we see in figures 2(b) and (c). In figure 2(b) we observe the PDF of $\sigma(\kappa = 1)$ for two different realizations (solid curve) and $\sigma(\kappa = 2)$ (dashed curve). In figure 2(c) we display $\sigma(\kappa = 3)$, $\sigma(\kappa = 4)$, $\sigma(\kappa = 30)$, $\sigma(\kappa = 40)$ (solid curves). To a large extent, the plots in figure 2(c) are indistinguishable from each other. In this figure, we observe that a hyperbolic PDF curve (short dashed curve) approximates the aforementioned PDF for $\sigma(\kappa = 40)$. In figure 2(c) $\sigma(\kappa = 2)$ (long dashed curve) is displayed for comparison.

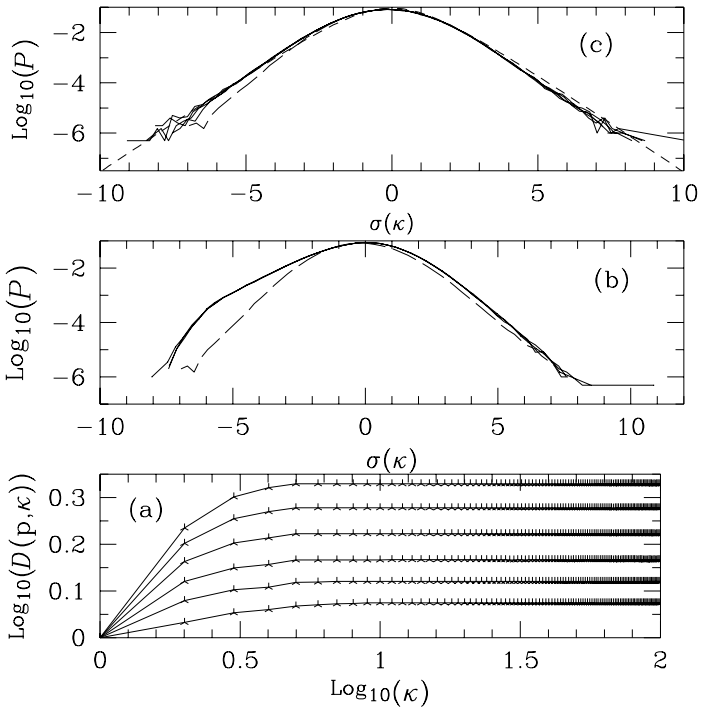

Figure 2. (a) Plot of $\log_{10} D(p, \kappa)$ versus $\log_{10} \kappa$ for different p. (b) Plot of $\log_{10} P$ versus $\sigma(\kappa)$ for $\kappa = 1$ (solid curve) and $\kappa = 2$ (dashed curve). (c) The same as (b) but for $\kappa = 3, 4, 30, 40$ (solid curve), $\kappa = 2$ (long dashed curve) and the corresponding hyperbolic PDF fit (short dashed curve).

3.2. The other sections at $\tau \neq 0$

Now, we will show that the PDFs for $\log_{10}(H_n)$ and $\sigma(\kappa)$ for different κ can be substantially different from those PDFs at $\tau = 0$. As τ becomes larger than $\tau = 0$, the 1D arrays on average become more disordered in space. The extent of order is measured in terms of the Kuramoto order parameter $R(t)$, which is defined as $R(t) = \left(\left|\sum_{j=1}^{j=N} \exp(\mathrm{i}\alpha_j)\right|\right)/N$, where $\alpha_j = \theta_{j+1}(t) - \theta_j(t)$. It is also said that $R(t)$ measures the phase coherence. In particular, if $R(t) = 1$, all the oscillators are in phase. When $R(t) = 0$, the phases α_i are typically distributed uniformly between 0 and 2π. As the 1D array evolves in time, a succession of spatially coherent and incoherent structures arises [6]. In figure 3(a) we observe the evolution of $R(t)$. Typically, the largest (smallest) extent of disorder in the 1D arrays, which occurs when $R(t)$ reaches a minimum (maximum), correlates with the largest (smallest) distances $H(t)$ between the two 1D arrays. The PDF for the TS of $\log_{10}(H_n)$ and $\sigma(\kappa = 40)$ for different values of τ are shown in figures 3(b) and (c), respectively. In figure 3(b) we observe that the PDF for $\log_{10}(H_n)$ at $\tau = 0.1$ (solid curve) can barely be described by a hyperbolic PDF. Instead, the right tail of the PDF for $\tau = 0.2$ (short dashed curve) must be described using two consecutive power laws. One of these extends over four orders of magnitude while the other spreads over three orders of magnitude. When $\tau = 0.47$ (long dashed curves), typically $R(t)$ is close to its local minima. For this value of τ, the right tail of the related PDF seems to have a faster decay than a hyperbolic PDF. In figure 3(c), we display the PDF of $\sigma(\kappa = 40)$ for different values of τ. The PDF for $\tau = 0.1$ (solid curve) can still be largely

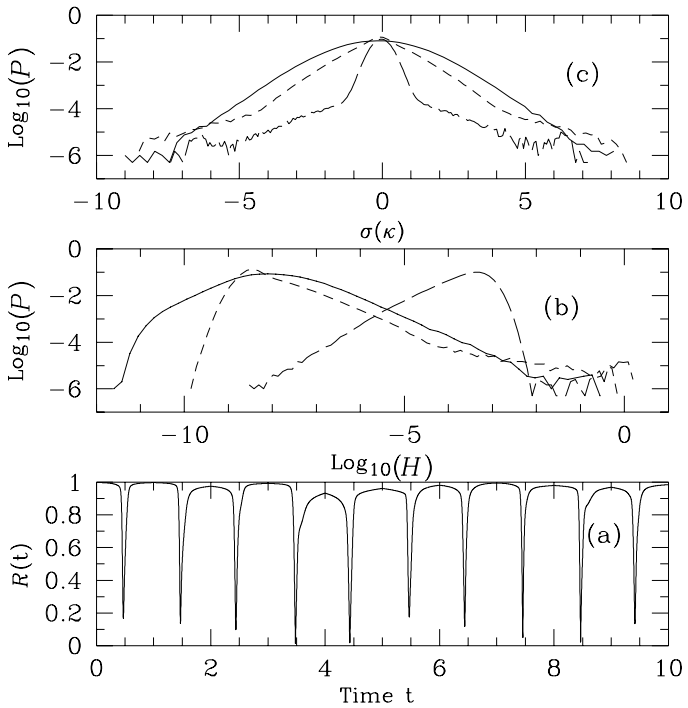

Figure 3. (a) Plot of $R(t)$ versus time t for $\Gamma = 17$ and $\beta = 20$. (b) Plot of $\log_{10} P$ versus $\log_{10} H_n$ for $\tau = 0.1$ (solid curve), $\tau = 0.2$ (short dashed curve) and $\tau = 0.47$ (long dashed curve). (c) Plot of $\log_{10} P$ versus $\sigma(\kappa)$ for $\tau = 0.1$ (solid curve) $\tau = 0.2$ (short dashed curve) and $\tau = 0.3$ (long dashed curve).

described by a hyperbolic PDF. However, those PDFs for $\tau = 0.2$ (short dashed curve) and for $\tau = 0.3$ (long dashed curve) have left and right tails that have to be described using at least two consecutive power-law functions. The reason for this lies in the τ-dependent separation that nearby trajectories undergo when $R \sim 0$. Now we consider the correlation dimension of the TS $\log_{10}(H_n)$. We do not find any clear-cut scaling region in figure 4(a). In this figure, the smallest slope in absolute value corresponds to an embedding dimension of two. The next largest slope in absolute value corresponds to an embedding dimension of three, and so on. Figure 4(a) suggests that this correlation dimension is no smaller than six.

3.3. Distribution of the laminar phases

Now we show that the features of the laminar phases in the present model deviate from those models of chaotic synchronization where on–off intermittency sets in [2]. It has been found in these studies that the distribution of the laminar phase duration l obeys the $l^{-3/2}$ power law [2]. This distribution law is derived from the related linearized differential equations [2]. In these studies, in order to characterize the laminar phase duration in the series H_n, it is necessary to take a threshold value η such that if $H_n < \eta$, the series H_n is in the laminar phase.

In figure 4(b) we observe the PDF of l for the TS H_n at $\tau = 0$ for different values of the threshold η. The cores of the PDF $P(l)$ can be approximated by exponential distributions for all these threshold values η. This is in contrast to the TS H_n at $\tau = 0.47$, where the 1D arrays show small coherence, i.e. $R(t) \ll 1$. In this case, the PDF $P(l)$ shows a power-law behaviour

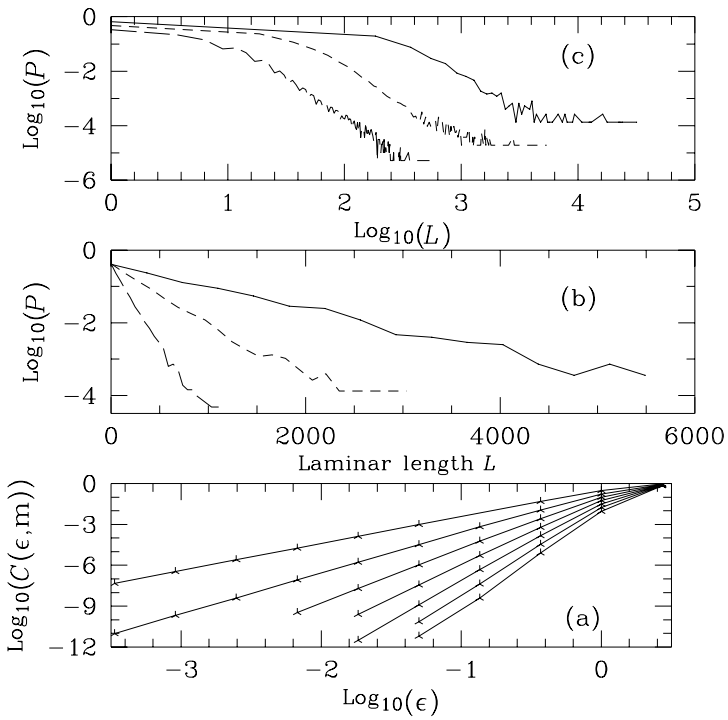

Figure 4. (a) Plot of the correlation dimension $\log_{10}(C(\epsilon, m))$ versus ϵ for different values of embedding m. (b) Plot of $\log_{10} P$ versus the laminar length L of the TS H_n at $\tau = 0$ for different thresholds. (c) The same as (b) but for $\tau = 0.47$ for different thresholds.

over some range of laminar values l for a given range of threshold values η. This is shown in figure 4(c). This is reminiscent of the PDF $P(l)$ found in models where on–off intermittency arises [2]. With respect to the case when $\tau = 0$, it is worth mentioning that there is a mechanism for intermittency in systems with symmetry, as in our model, which is caused by small additive noise or periodic perturbations in systems that have homoclinic attracting orbits. This system has been studied by Stone and Holmes [9]. They have shown that the distribution of the length of the laminar phases has an exponential tail in contrast to on–off intermittency, where the distribution of the length of the laminar phases has a power-law tail [9].

4. Conclusions

In this paper, we have studied a model of two coupled identical 1D arrays of phase oscillators at the threshold of complete synchronization. The 1D arrays are driven periodically and show STC. Many statistical properties of the TS H_n of this system depend on the sampling section τ. For large coupling Γ, we have found that it is possible to describe the PDF of $\log_{10} H_n$ with hyperbolic distributions for the section $\tau = 0$. This implies that the tails of the PDF for H_n behave as truncated Levy laws. For other sections $\tau \neq 0$, we have found that the tails of the PDF for H_n can be described with two consecutive power laws or with even faster decays. A similar situation occurs for the TS of the rates of change $\sigma(\kappa) = \log_{10}(H_{n+\kappa}/H_n)$. The PDF of $\sigma(\kappa)$ quickly tends to a limit as κ increases. In fact for $\kappa \sim 4$, this limit is almost reached. The autocorrelation function of the TS H_n decays exponentially fast, or even faster

than exponential depending on the section τ. We have found that the correlation dimension of the TS H_n is no smaller than six. Possibly this supports the fact that our TS H_n behaves to some extent like noise. The PDF of the laminar phases depends strongly on the section τ. We find that these distributions can be exponential or even follow a power law. This suggests that these PDF could be described in terms of the Tsallis statistics [10].

Acknowledgments

This work was also supported by CONACYT-México. I am also grateful for support from the IFUAP-Medusa computer facilities.

References

[1] Ott E 1993 *Chaos in Dynamical Systems* (Cambridge: Cambridge University Press)
[2] Fujisaka H and Yamada T 1983 *Prog. Theor. Phys.* **69** 32
Afraimovich V S, Verichev N N and Rabinovich M I 1986 *Radiophys. Quant. Electron* **29** 795
Pecora L M and Carroll T L 1990 *Phys. Rev. Lett.* **64** 821
Heagy J F, Platt N and Hammel S M 1994 *Phys. Rev.* E **49** 1140
[3] Fujisaka H and Yamada T 1985 *Prog. Theor. Phys.* **74** 918
Yu L, Ott E and Chen Q 1990 *Phys. Rev. Lett.* **65** 2935
Fujisaka H *et al* 1997 *Phys. Rep.* **290** 27
[4] Special issue 1996 *Chaos* **6** (3)
Special issue 1997 *Chaos* **7** (4)
Kittel A, Parisi J and Pyragas K 1999 *Handbook of Chaos Control* ed H G Schuster (New York: Wiley)
[5] Pikovsky A and Kurths J 1994 *Phys. Rev.* E **49** 898
Kocarev L and Parlitz U 1996 *Phys. Rev. Lett.* **77** 2206
[6] Pando L C L 2000 *Phys. Lett.* A **273** 70
[7] Afraimovich V S *et al* 1994 *Stability, Structures and Chaos in Nonlinear Synchronization Networks* (Singapore: World Scientific)
Hasegawa A, Endo T and Komuro M 2000 *Electronics and Communications in Japan: Part II. Electronics* **83** 26 and references therein
[8] Sornette D 2000 *Critical Phenomena in Natural Sciences* (Berlin: Springer)
[9] Stone E and Holmes P 1990 *SIAM J. Appl. Math.* **50** 726
Stone E and Holmes P 1991 *Phys. Lett.* A **155** 29
[10] Tsallis C 2001 Private communication